Photonic nanojet array for fast detection of single nanoparticles in a flow

Hui Yang, Matteo Cornaglia and Martin A.M. Gijs*

Laboratory of Microsystems, École Polytechnique Fédérale de Lausanne, 1015 Lausanne, SWITZERLAND

ABSTRACT:

We detect by optical microscopy Au and fluorescent nanoparticles (NPs) during their motion in water-based medium, using an array of dielectric microspheres that are patterned in a microwell array template. The microspheres act as lenses focusing the light originating from a microscope objective into so-called photonic nanojets that expose the medium within a microfluidic channel. When a NP is randomly transported through a nanojet, its back-scattered light (for a bare Au NP) or its fluorescent emission is instantaneously detected by video microscopy. Au NPs down to 50 nm in size, as well as fluorescent NPs down to 20 nm in size, are observed by using a low magnification/low numerical aperture microscope objective in bright-field or fluorescence mode, respectively. Compared to the NPs present outside of the photonic nanojets, the light scattering or fluorescence intensity of the NPs in the nanojets is typically enhanced by up to a factor ~40. The experimental intensity is found to be proportional to the area occupied by the NP in the nanojet. The technique is also used for immunodetection of biomolecules immobilized on Au NPs in buffer and, in future, it may develop into a versatile tool to detect nanometric objects of environmental or biological importance, such as NPs, viruses or other biological agents.

KEYWORDS: Photonic nanojet, microfluidics, microsphere, microlens, nanoparticle

Recently considerable interest arose for high-resolution sensing systems that can detect nano-objects and even individual molecules in liquids [1,2]. Advanced optical techniques have been proposed for sensitive detection of nano-objects, but required high-end, expensive, and bulky experimental setups [3,4]. If direct optical detection of NPs in liquids would be possible using a standard microscope, this could lead to more affordable and portable sensing applications. However, conventional optics only permits detecting relatively large objects, because the scattered light intensity decreases with decreasing size and the light collection capability of a standard microscope objective is limited by its numerical aperture (NA) [5]. Therefore only NPs that are either larger than several hundred nanometers or having extremely enhanced scattering probability can be detected.

While a microsphere is known to act as a focusing microlens [6,7,8,9], when it has a refractive index contrast relative to the fluid medium that is less than 2:1 and a diameter between several to tens of wavelengths (λ), a highly-focused propagating beam from the shadow-side surface of the microsphere is generated due to constructive interference of the light field [10,11]. This beam is termed as "photonic nanojet" and has a sub-λ full-width-at-half-maximum (FWHM) transverse dimension and typically is several λ in length [11,12]. A very interesting predicted property of a photonic nanojet is that the presence of a particle, much smaller than λ and positioned within the nanojet, significantly enhances back-scattering of the light through the microsphere [13,14]. High-refractive index microspheres embedded in a polydimethylsiloxane (PDMS) medium containing dispersed 50 nm size Au NPs confirmed a back-scattering intensity two times larger than that caused by the isolated microsphere itself indeed [15,16]. If appropriate microspheres could be integrated into microfluidic devices for direct detection of objects with a dimension much smaller than λ, this could be of high interest for many environmental and biological sensing applications.

We positioned at the bottom of a microfluidic channel an array of microspheres, which were self-

assembled in a microfabricated Parylene-C template on a glass substrate, and illuminated the chip by an optical microscope for generation of the photonic nanojets in the microfluidic medium (see Figure 1a). Experimental details are given in the Supporting Information; briefly, 3 μm-size melamine microspheres were selected due to their high refractive index, low light absorbance, and optimum light focusing capability in water [12]. We performed a finite element method (FEM) study on the electromagnetic wave propagation through the system and the water medium to investigate the light intensity distribution in the vicinity of the microlens array (see Figure 1b(i), details described in the Supporting Information). The photonic nanojet is developed ~1 μm above the top surface of the microsphere and the light intensity along the microsphere focal plane in Figure 1b(ii) indicates a FWHM of ~240 nm. Figure 1c depicts the working principle of our technique. If the size of a nano-object that transits through a photonic nanojet is smaller than FWHM, only a portion of the illuminating light is back-scattered (see Figure 1c(i)). With increasing size of the nano-object, the intensity of the scattered light increases, until the object back-scatters all light gathered by the microsphere, when its size equals FWHM (see Figure 1c(ii)). For even bigger objects (see Figure 1c(iii)), the retro-reflected light recorded by the microscope does not further increase and the signal saturates. In our experiments, the largest NPs we used were 400 nm Au and 460 nm fluorescent NPs (see further), both sizes being well above the FWHM of the nanojet. By using an array format for the microlenses, the same NP can be transported through a sequence of photonic nanojets placed in the same flow stream. The optical signal obtained from a row of lenses is then easily correlated to unambiguously prove the transit of even a single moving NP. Another advantage of using an array is that a larger region of the microfluidic channel is probed, which is advantageous for detecting low NP concentrations.

First the potential of our technique in bright-field microscopy was investigated by detecting Au NPs, as they are important in chemistry, physics and biology [17,18,19]. Au NPs in the 50-400 nm range were dispersed in de-ionized water and introduced into the microfluidic channel at a flow velocity of ~10 μm/sec. Figure 2a(i,ii) show that the presence of a 400 nm or 200 nm Au NP in

the nanojet results in a back-scattered light intensity that is significantly enhanced with respect to that of a NP outside of the nanojet (see also Movie 1 of the Supporting Information). Figure 2(iii-v) show the results obtained from 100 nm, 80 nm and 50 nm Au NPs, respectively; direct optical microscopy (without the microspheres) cannot resolve these NPs. Figure 2a(vi) is a plot of the experimental back-scattered light intensity as function of the NP size, indicating an initial rise followed by a saturated behavior. The full curve plots the ratio between the area of the maximum cross section of an Au NP ($=\pi \cdot R_{NP}^2$, with R_{NP} the radius of the NP) and the transverse focal area of the nanojet ($=\pi \cdot r^2$, r=FWHM/2=120 nm, as obtained from the simulation in Figure 1b), essentially confirming the detection principle of Figure 1c. For comparison, the signal from a 400 nm and 200 nm Au NP moving outside of the microsphere region was plotted in Figure 2a(vi), and, when using the microsphere, a signal enhancement factor of ~40 and ~8 was observed for a 200 nm and 400 nm Au NP, respectively (the latter value is smaller because the NP is larger than the nanojet (see Figure 1c(iii)). The details on the data processing to obtain these enhancement factors are described in the Methods.

We further tested our technique by using calibrated polystyrene fluorescent NPs with emission wavelength λ_{em} = 515 nm (see Figure 2b). NPs with size from 20 nm to 460 nm were dispersed in phosphate buffered saline (PBS)-Tween 20 (0.5% v/v) solution and introduced into the microfluidic channel. Figure 2b(i-v) show the experimental results for NPs with diameter of 460 nm, 190 nm, 110 nm, 46 nm, and 20 nm, respectively. When a fluorescent NP passed through a photonic nanojet, its fluorescent excitation was highly enhanced (see also Movie 2 of the Supporting Information). For the used flow conditions, the NPs were typically exposed to the strong optical field in the nanojet for 20 milliseconds. Thanks to the use of a microsphere, a signal enhancement factor of ~44 and ~6 was observed for a 190 nm and 460 nm fluorescent NP, respectively (details on the data processing are described in the Methods). The fluorescent emission of the NPs was extremely bright, so that NPs with 20 nm in diameter could be still distinguished when passing through a nanojet, as the fluorescent emission filter efficiently

4

removed the excitation light and fluorescence at wavelengths other than λ_{em}. Figure 2b(vi) is a plot of the experimental fluorescent emission intensity as function of the NP size, indicating an initial rise followed by a saturated behavior, and compared to the same model as in Figure 2a(vi). It should be noted that both the exact position of a NP within a nanojet and its flow velocity in the microfluidic channel potentially can induce variations in the detection signal (see Supporting Information). In our experiments, in order to avoid these variations, only the images in which the NPs in the nanojets showed maximum intensities were used for data processing. In this case, the NPs were aligned at the minimum transverse dimension of the photonic nanojet and the velocity of these particles was set to 10 μm/s, so that a variation in the detection signal was only due to NPs with different sizes or optical properties.

We then demonstrated the potential of our technique for immunofluorescent detection. A general advantage of using nanomaterials in an immunoassay is their high specific surface, enabling the immobilization of significant amounts of ligands (antibodies) that can specifically interact with receptors (antigens) in the sample [20]. Within the group of noble metal NPs, Au NPs are mostly used for biosensor applications [20,21] due to their biocompatibility and their relatively simple production and modification [22]. We functionalized Au NPs of different size with a monolayer of 6-mercaptohexanoic acid via thiol linkages. The thus functionalized Au NPs were conjugated with biomolecules via peptide bonds using N-ethyl-N'-(3-dimethylaminopropyl)carbodiimide hydrochloride and N-hydroxysulfosuccinimide as mediators. Details on the experimental protocol of Au NPs modification and biomolecular conjugation are described in the Supporting Information. Briefly, two experimental protocols were performed, first Atto488-labeled biotin was covalently linked with surface-modified Au NPs (see Figure 3a(i)), and secondly we performed an one-site immunoassay by conjugating surface-modified Au NPs with normal mouse IgG, followed by exposure to AlexaFluor647-labeled anti-mouse IgG detection antibodies (see Figure 3b(i)). For the two assay protocols, the conjugated Au NPs showed an enhanced fluorescence, when the functionalized Au NPs were transiting through a nanojet. For example,

the light intensity profiles along the cross section of the fluorescent Au NPs present in and outside of a nanojet are shown in Figure 3a(ii-iii) and 3b(ii-iii), respectively. These results indicate that the detection of biomolecules with weak optical signal intensities can be very efficiently enhanced indeed by the microlens array due to the highly amplified fluorescent excitation field in the photonic nanojet.

In conclusion, we achieved the detection of NPs with a size far below the classical diffraction limit in a microfluidic device by using a conventional bright-field and fluorescence microscope. In contrast to optical detection-based analytical techniques, such as those that use laser excitation and light scattering, which demonstrated detection of NPs in a solution down to a size of 30 nm [4], our technique does not rely on complex experimental setups and has the ability to easily distinguish individual NPs and do live counting of these NPs by using a standard microscope set-up. The microscope objective was used in combination with a dielectric microsphere array to generate an array of photonic nanojets. When NPs were transported by a flowing medium through a nanojet, their light scattering or fluorescence intensity was typically enhanced by a factor ~40. We also verified that immunocomplexes formed on Au NPs can be detected via this method. Overall, as the intensity of the scattered or fluorescent signal generated by the NP in the nanojet depends on the size of the NP, size-dependent detection of nano-objects in a solution might be envisaged in future. Also for the used flow conditions, the typical transit time of a NP through a photonic nanojet is ~20 millisecond, which allows rapid detection of a representative number of NPs by the ability of detecting many single transit events. In future, slower flow rates or application of a smaller translational velocity of the microsphere array with respect to a sample might result in longer measurement times for detecting even smaller NPs or weaker fluorescent signals. Therefore, we believe that our technique that dynamically exploits the unique properties of a photonic nanojet could evolve in a tool to detect a wide class of nano-objects, such as proteins, viral particles, or for monitoring synthesis and aggregation processes on a molecular level.

METHODS

We used carboxyl-functionalized melamine microspheres (Sigma-Aldrich, 3 μm in diameter, standard deviation < 0.1 μm) as the microlenses. The microsphere array was realized by fabricating first a Parylene-C well template on a glass substrate by standard cleanroom processes. Next the microspheres were suspended in a patterning solution with pH of 2, made by mixing PBS buffer with HCl (25% original, 0.2% v/v in PBS). A droplet of the patterning buffer was transported over the microwell array for 10 patterning cycles (1 cycle = 1 passage of the droplet). A microsphere loading efficiency >99% was achieved. The glass substrate was then ready for clamping to a PDMS half-channel, which was replicated from a SU-8 structure that was fabricated on a silicon wafer. A 5:1 mixture of PDMS prepolymer and curing agent (Dow Corning) was cast over the SU-8 mold and cured at 70 °C for overnight. Then the PDMS replica was peeled off from the mold, resulting in a microfluidic half-channel with a height of 20 μm, a width of 800 μm and a length of 24 mm. Two polymethylmetacrylate plates were used to clamp the PDMS replica and the glass chip with the Parylene-C microwell array containing the microlenses.

Bare Au NPs in citrate buffer (Sigma-Aldrich) were diluted in de-ionized water, and calibrated yellow-green fluorescent (excitation at 505 nm/emission at 515 nm, Molecular Probes) NPs were dispersed in PBS-Tween 20 (0.5% v/v) buffer into the same concentration of 1×10^5 particles/mL. All solutions were introduced into the microfluidic channel at a flow velocity of ~10 μm/sec by a neMESYS syringe pump (Cetoni, Germany) for ~ 30 min. A sample amount of ~ 300 nL was used in each experiment. After the conjugation of biomolecules on the Au NPs (details described in the Supporting Information), the fluorescent molecule-conjugated Au NPs were spiked in PBS buffer and introduced into the microfluidic channel with the same flow

velocity and amount of sample used for all experiments. During the sample preparation procedure, the stock solutions of the Au NPs are mixed thoroughly by a rotary mixer before being diluted with DI water in successive steps into a final concentration of 1×10^5 particles/mL. Therefore, for all Au NPs, the stock solution is at least diluted 1900 times. Therefore the amount of citrate buffer in the final sample solution is minor.

An Axiovert S100 (Carl Zeiss) inverted microscope, equipped with a 20× objective with NA of 0.22 (Zeiss Objective LD EC Epiplan-Neofluar 20×/0.22 DIC M27, 422452-9900), was used for illumination and signal detection. The microscope was configured with a mercury vapor arc lamp (X-Cite 120, Carl Zeiss) and appropriate fluorescent filter sets. Image acquisition and light detection were achieved using a CCD camera (ORCA-C4742-80ER, Hamamatsu Photonics). The integration time for recording an image was set to 20 milliseconds, which was determined by the flow velocity (~10 μm/sec) and the FWHM of the photonic nanojet (~240 nm). This integration time was just long enough to record the signal intensity of the NP during its full transit at the best focused part of the nanojet.

The normalized light intensity data of Figure 2a(vi) and 2b(vi) for the Au and fluorescent NPs situated in the nanojet were obtained by integrating the intensity over the microsphere area in presence of a NP and subtracting the integrated intensity from the same area when no NP was present, followed by normalization of this background-corrected integrated intensity by the background-corrected integrated intensity of a 400 nm Au NP or a 460 nm fluorescent NP located in the nanojet, respectively. For the experimental points obtained for the Au and fluorescent NPs situated outside of the microsphere area, the normalized light intensity is obtained in a similar way, but normalization is still done by the integrated light intensity of a 400 nm Au and 460 nm fluorescent NPs situated in the nanojet, respectively. The signal enhancement factors of the 400 nm and 200 nm Au NPs, as well as of the 460 nm and 190 nm fluorescent NPs were obtained by dividing the thus obtained normalized light intensity from a NP in the nanojet by that obtained

from a NP out of the nanojet.

ASSOCIATED CONTENT

Supporting Information

Technical information and figures on the device fabrication, microlens effect of the dielectric microspheres. Details on the numerical simulation of the microlens array and surface-modification and biomolecule conjugation on Au NPs. There are also further discussions on the detection of nano-objects in a microfluidic channel and on the influence of the position of a NP in the photonic nanojet and flow velocity on the detection signal. This material is available free of charge via the Internet at http://pubs.acs.org.

AUTHOR INFORMATION

Corresponding Author

*E-mail: hui.yang@epfl.ch

Notes

The authors have an International Patent Application (provisional number PCT/IB2014/063747) entitled "System for optical detection and imaging of sub-diffraction-limited nano-objects" for the device described in this work.

ACKNOWLEDGMENT

REFERENCES

[1] Anker, J. N.; Hall, W. P.; Lyandres, O.; Shah, N. C.; Zhao, J.; Van Duyne, R. P. *Nat. Mater.* **2008**, 7, 442-453.

[2] Maxwell, D. J.; Taylor, J. R.; Nie, S. *J. Am. Chem. Soc.* **2002**, 124, 9606-9612.

[3] Vollmer, F.; Arnold, S. *Nat. Methods* **2008**, 5, 591-596.

[4] Zhu, J.; Ozdemir, S. K.; Xiao, Y.-F.; Li, L.; He, L.; Chen, D.-R.; Yang, L. *Nature Photon.* **2010**, 4, 46-49.

[5] Yang, H.; Moullan, N.; Auwerx, J.; Gijs, M. A. M. *Small* **2014**, 10, 1712-1718.

[6] Brody, J. P.; Quake, S. R. *Appl. Phys. Lett.* **1999**, 74, 144-146.

[7] Domachuk, P.; Cronin-Golomb, M.; Eggleton, B. J.; Mutzenich, S.; Rosengarten, G.; Mitchell, A. *Opt. Express* **2005**, 13, 7265-7275.

[8] Wenger, J.; Gérard, D.; Aouani, H.; Rigneault, H. *Anal. Chem.* **2008**, 80, 6800-6804.

[9] Schwartz, J. J.; Stavrakis, S.; Quake, S. R. *Nat. Nanotechnol.* **2010**, 5, 127-132.

[10] Lee, S.; Li, L.; Wang, Z. *J. Opt.* **2014**, 16, 015704.

[11] Heifetz, A.; Kong, S.-C.; Sahakian, A. V.; Taflove, A.; Backman, V. *J. Comput. Theor. Nanosci.* **2009**, 6, 1979-1992.

[12] Yang, H.; Gijs, M. A. M. *Anal. Chem.* **2013**, 85, 2064-2071.

[13] Li, X.; Chen, Z.; Taflove, A.; Backman, V. *Opt. Express* **2005**, 13, 526-533.

[14] Chen, Z.; Taflove, A.; Li, X.; Backman, V. *Opt. Lett.* **2006**, 31, 196-198.

[15] Zhao, L.; Ong, C. K. *J. Appl. Phys.* **2009**, 105, 123512.

[16] Yang, S.; Taflove, A.; Backman, V. *Opt. Express* **2011**, 19, 7084-7093.

[17] Cognet, L.; Lounis, B. *Gold Bull.* **2008**, 41, 139-146.

[18] Kreibig, U.; Vollmer, M. *Optical properties of metal clusters*; Springer, 1995.

[19] Eustis, S.; El-Sayed, M. A. *Chem. Soc. Rev.* **2006**, 35, 209-217.

[20] Holzinger, M.,; Goff, A. L.; Cosnier, S. *Front. Chem.* **2014**,
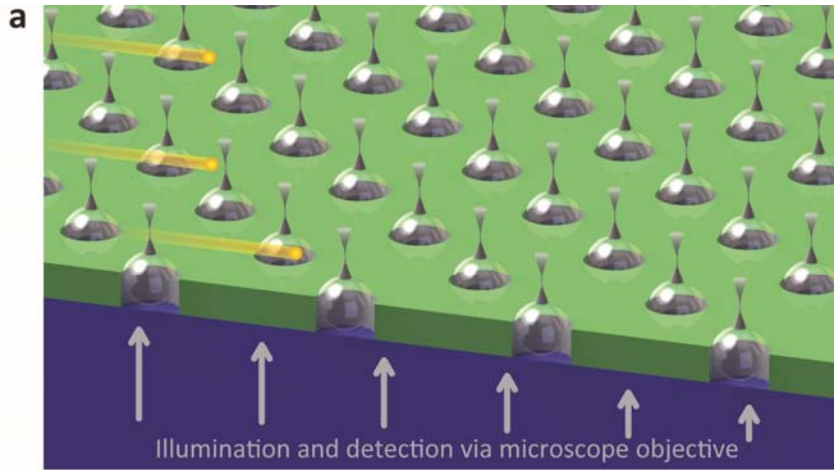
doi:10.3389/fchem.2014.00063.

21   Li, Y.; Schluesener, H. J.; Xu, S. *Gold Bull.* **2010**, 43, 29-41.

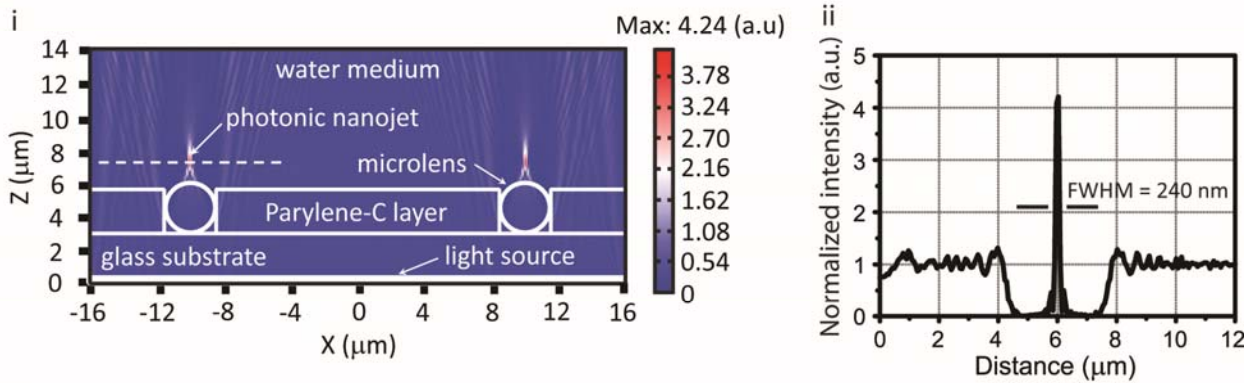22   Biju, V. *Chem. Soc. Rev.* **2014**, 43, 744-764.

Figure 1. Schematic illustration of the optical detection of NPs. (a) Dielectric microspheres are patterned in a microfabricated well template on a glass substrate and an optical microscope with low-NA objective is placed beneath the thus formed microlens array. Illumination light from the objective is focused by each microlens into a photonic nanojet having a sub-diffraction limit beam width. When a NP, randomly dispersed in a water-based medium, is transported through a nanojet, its back-scattered light is instantaneously detected via the microscope objective. (b) FEM simulation of the light propagation through the glass substrate, the Parylene-C well template and the dielectric microspheres in water medium. (i) 2D simulation showing the photonic nanojet emerging from the microspheres (λ=400 nm); (ii) intensity distribution along the dashed line in (i), showing a FWHM of the nanojet of 240 nm. (c) Detection principle of the scattered/emitted light from a NP transported in a PDMS microfluidic structure. (i) The NP is smaller than the transverse dimension of the photonic nanojet and part of the illumination light is back-scattered; (ii) the NP has the same size of the photonic nanojet and all of the light focused by the microsphere is back-scattered; (iii) the NP is bigger than the nanojet and the back-scattered light is not further enhanced.

Figure 2. Detection of Au and fluorescent NPs during their motion through a nanojet. (a) Backscattering intensity from Au NPs under white-light illumination. (i-v) Microscopic images (left column) and intensity profiles along the dashed lines in the left panels (right column) for Au NPs of decreasing size. Due to their size, Au NPs of 400 nm (i) and 200 nm (ii) are also detectable when they are outside a nanojet, and their intensity profile is plotted on the corresponding right panels too. (vi) Back-scattered light intensity of Au NPs, positioned within and outside of a nanojet, as function of the NP size and normalized by the intensity of the 400 nm Au NP in the nanojet. The full curve corresponds to a simple geometrical model, in which the back-scattered light is proportional to the area of a NP placed in the nanojet; this area is limited to and normalized by the simulated cross-section of the nanojet. Points represent the average from 20 measurements, error bars the variance. (b) Emission at λ_{em}=515 nm of fluorescent NPs when excited at a wavelength of λ_{ex}=505 nm. (i-v) Microscopic images (left column) and intensity profiles along the dashed lines in the left panels (right column) for fluorescent NPs of decreasing size. Fluorescent NPs of 460 nm (i), 190 nm (ii), and 110 nm (iii) are also detectable when they are outside a nanojet, and their intensi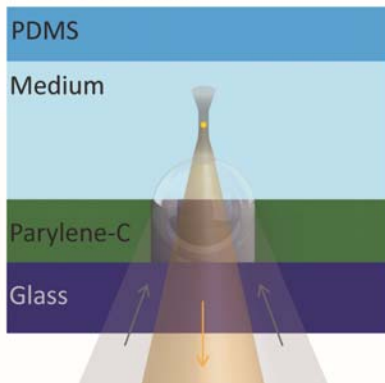ty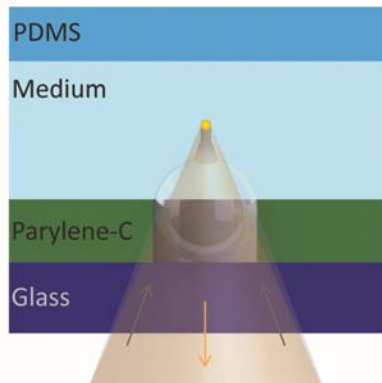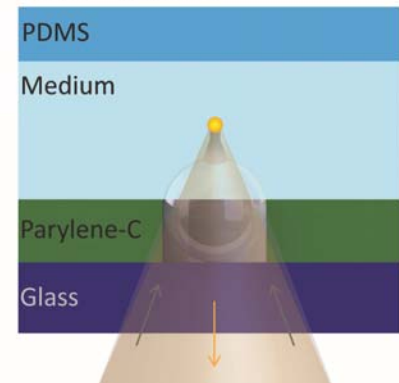 profile is plotted on the corresponding right panels too. (vi) Fluorescent intensity of the NPs, positioned within and outside of a nanojet, as function of the NP size and normalized by the intensity of the 460 nm fluorescent NP in the nanojet. The full curve corresponds to a geometrical model, in which the fluorescent intensity is proportional to the area of a NP placed in the nanojet; this area is limited to and normalized by the simulated cross-section of the nanojet. Points represent the average from 20 measurements, error bars the variance.

Figure 3. Fluorescent detection experiments using Au NPs. (a) Direct detection of Atto488-labeled biotin spiked in PBS. (i) Schematic conjugation protocol of the biotin to functionalized Au NPs. (ii,iii) Microscopic images (left column) and intensity profiles along the dashed lines in the left panels (right column) for fluorescently labeled Au NPs of 400 nm and 200 nm, respectively. These particles are also detectable when they are outside a nanojet, and the latter intensity profile is plotted on the corresponding right panels too. (b) Detection of mouse IgG on functionalized Au NPs using AlexaFluor647-labeled anti-mouse IgG detection antibodies, all spiked in PBS. (i) Schematic two-step conjugation protocol for detection of mouse IgG by functionalized Au NPs. (ii,iii) Microscopic images (left column) and intensity profiles along the dashed lines in the left panels (right column) for fluorescently labeled Au NPs of 400 nm and 200 nm, respectively. These particles are also detectable when they are outside a nanojet, and the latter intensity profile is plotted on the corresponding right panels too.

a

Illumination and detection via microscope objective

b

i

Max: 4.24 (a.u)

water medium

photonic nanojet

microlens

Parylene-C layer

glass substrate

light source

ii

FWHM = 240 nm

c

i. NP < nanojet

PDMS
Medium
Parylene-C
Glass

ii. NP = nanojet

PDMS
Medium
Parylene-C
Glass

iii. NP > nanojet

PDMS
Medium
Parylene-C
Glass

a

i

ii

iii

iv

v

vi

b

i

ii

iii

iv

v

vi